High-Resolution In-Situ Structural Measurements of the $Li_{4/3}Ti_{5/3}O_4$ "Zero-Strain" Insertion Material

F. Ronci, P. Reale, B. Scrosati, and S. Panero

Dipartimento di Chimica, Università "La Sapienza", P.le Aldo Moro, 5-00186 Roma, Italy

V. Rossi Albertini* and P. Perfetti

Istituto di Struttura della Materia, Area di ricerca di Tor Vergata del CNR, Via del Fosso del Cavaliere, 100-00133 Roma, Italy

M. di Michiel and J. M. Merino

European Synchrotron Radiation Facility, Polygone Scientifique "Louis Néel", Rue Jules Horowitz, 6-38000 Grenoble, France

Received: August 20, 2001; In Final Form: December 31, 2001

In-situ X-ray diffraction studies have been performed on a $Li_{4/3}Ti_{5/3}O_4$ electrode upon cycling in a Li cell, by using a very high energy (87.5 keV) synchrotron beam. The real time structural changes of its crystalline lattice were observed over two complete cycles of the cell. The high-resolution measurements allowed us to precisely monitor the extremely small breathing movement of the structure and to plot the curve of the lattice parameter as a function of the lithiation degree. The investigation revealed an unexpected behavior in the structural evolution upon cycling, which was attributed to the reversible passage from a monophasic to a biphasic domain upon insertion. Furthermore, the structural evolution turned out to be slightly different in the first and in the second cycle. This suggests that irreversible rearrangements, like the ones observed for every other insertion compound, occur also in this case, although on an extremely smaller scale.

Introduction

The lithium spinel titanate $Li_{4/3}Ti_{5/3}O_4$ is a promising negative electrode for Li-ion cells. It is a member of the $Li_{1+y}Ti_{2-y}O_4$ family ($0 < y < 1/3$), also studied for their superconductivity properties. In particular, $LiTi_2O_4$ was the first discovered superconductor having $T_C > 10$ K.[1]

The electrochemical properties of $Li_{4/3}Ti_{5/3}O_4$ are characterized by a Li^+ insertion process that involves one equivalent per formula unit (i.e., $0 < x < 1$ in $Li_{4/3+x}Ti_{5/3}O_4$, where x is the insertion degree) with constant discharge and charge potentials close to 1.56 V vs $Li^+/Li°$. Such a working potential is quite high for a negative-electrode material, but it has the advantage of being inside the electrochemical stability window of the most common electrolytes, this concurring in making this electrode suitable for prolonged cyclability.[2] Furthermore, the use of $Li_{4/3}Ti_{5/3}O_4$ coupled with a high-voltage cathode in a lithium-ion cell was recently proposed.[3]

The insertion process in $Li_{4/3}Ti_{5/3}O_4$ is known to happen with negligible structural variations, a remarkable characteristic if one considers that structural stress is among the main causes of capacity fading in batteries. The presence of a voltage plateau in the whole insertion range, both in the discharge and in the charge processes, suggests the presence of a two-phase equilibrium. This fact was verified by Ohzuku et al.[4] by performing ex-situ X-ray diffraction on powders electrochemically inserted at different lithium insertion degrees. The two phases were resolved to be both spinel structures ($Fd\bar{3}m$ space group), differing only in the lithium ion sublattices: $[Li]_{8a}[Li_{1/3}Ti_{5/3}]_{16d}[O_4]_{32e}$ and $[Li_2]_{16c}[Li_{1/3}Ti_{5/3}]_{16d}[O_4]_{32e}$ in the Wyckoff formalism. The lithium ion occupancy of both tetrahedral (8a) and octahedral (16d) sites in the initial $Li_{4/3}Ti_{5/3}O_4$ phase was confirmed by ^{7}Li NMR[5] and ^{6}Li NMR measurements.[6]

The two-phase process was more recently confirmed by Sharner et al.[7] using ex-situ X-ray diffraction at high scattering angles and the difference of the a lattice parameters of the two spinel structures was quantified in being less than 0.1%, passing from 8.3595 to 8.3538 Å. Subsequently we reported[8] a method based on the EDXD (Energy Dispersive X-ray Diffraction) to perform in-situ time-resolved sampling of the evolving crystalline structure upon cycling and we applied this technique to the study of this titanate compound.[9] In such work, a first indication of the change of the a lattice parameter as a function of the insertion degree x was reported and the variation of the lattice parameter was found to be in a good agreement with the one reported by Scharner et al. Unfortunately, the precision of this laboratory technique (about 10^{-4} Å) was only 1 order of magnitude better than the total variation, so that the experimental values were affected by a remarkable statistical noise. Due to this limitation, only a linear approximation estimate of the actual shape of the a vs x curve could be obtained. However, these data seemed to show that the initial value of the lattice parameter was not matched back after the first cycle, suggesting the presence of partially irreversible effects, like the ones reported for ordinary insertion compounds.

In this paper we report on in-situ synchrotron radiation XRD performed on this compound at the ID15B beamline of the European Synchrotron Radiation Facility, to deepen and complete the results of the previous work.

* Author to whom correspondence should be addressed.

10.1021/jp013240p CCC: $22.00
Published on Web 03/06/2002

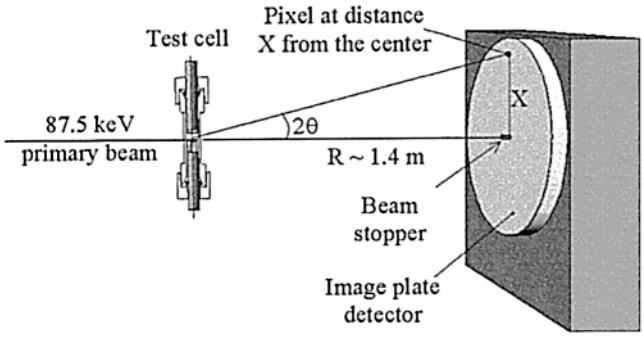

Figure 1. Sketch of the experimental setup. The cell is inclined by 1° degree with respect to the incident beam direction, to attain the grazing incidence condition that maximizes the irradiated area of the sample.

Experimental Section

The compound was synthesized in our laboratories using a solid-state method described elsewhere.[9] The electrode membrane was cast on an aluminum foil using the Doctor Blade technique. PVdF (Solvay Solef 6020), Super P (M. M. M. Carbon Belgium) and $Li_{4/3}Ti_{5/3}O_4$ powder were used, respectively, as binder, electronic conduction enhancer, and active material in a 12:5:83 weight ratio. After a drying procedure (12 h at 100 °C under vacuum), the membrane was brought inside a MBraun drybox with moisture and oxygen levels below 1 ppm, in which the test cell, described in detail in a previous work,[10] was assembled by using lithium metal as counter electrode and 1 M $LiClO_4$ in EC-DMC (1:1) as electrolyte.

The Experimental Setup. The experimental method consisted of collecting a sequence of diffractograms produced by the evolving lattice structure of the active material during the first two galvanostatic cycles of the test cell. The cell was cycled using an AMEL 545 galvanostat with a constant current equivalent to a C/10 rate in the 2.3−1.2 V range. Considering that ~105 s were necessary for collecting one pattern (20 s for the actual acquisition and ~85 s for data downloading), a total theoretical number of 548 patterns per cycle could be obtained. Such a high sampling rate was chosen in order to have an almost constant composition during a single scan. In fact, during 105 s the x variation in $Li_{4/3+x}Ti_{5/3}O_4$ is less than 0.004. Furthermore, in this way we had the possibility of detecting changes that occur in very small insertion ranges and to minimize the loss of structural information due to the unavailability of the beam during synchrotron refills and problems connected to it.

The experimental setup used for these measurements, schematically described in Figure 1, consisted of the use of a high energy (87.5 keV) monochromatic primary X-ray beam and of an image plate detector model MAR 345. The advantages of utilizing such a high-energy beam, connected to the almost total transparency of the cell to it, are reported in detail elsewhere.[11] They can be summarized as follows: (a) increase of the signal at the detector, (b) elimination of the difficulties arising from the asymmetric positioning of the cell, which otherwise would produce shaded areas on the image plate detector due to differential absorption.

In particular, the solution of the latter problem allows a complete radial integration of the Debye−Scherrer rings, improving enormously the statistics. Furthermore, a high-energy beam is diffracted at small angles. The consequent required increase of the sample-to-detector distance improves the scattering geometry.

To increase the signal-to-noise ratio, the largest possible area of the electrode must be irradiated. This induces a spread of the scattering angle values and a consequent decrease of the angular resolution, which can be compensated by the aforementioned increase of the sample-to-detector distance.

Another advantage is that the effect of the presence of higher harmonics (~262.5 keV), producing ghost peaks, is no longer visible. Indeed, harmonics of an 87.5 keV X-ray beam have a too high energy to be produced by the wiggler magnets with remarkable intensity. Morover their penetration ability is comparable with that of the fundamental while, at lower energies, they are much more penetrating (and, therefore, visible) than the fundamental. To this must be added that the detector efficiency drops dramatically above 100 keV, so that it acts as a low pass filter.

Finally, using such high energy radiation, the energy transfer from the incident beam to the HDPE cell walls is ruled mainly by the Compton effect, rather than by the photoelectric interaction, so that the radiation damage is much lower and no problem occurred even after long exposures.

All these reasons show that the system under study was in optimal experimental condition to be deeply investigated and to reveal even minimum variation of the lattice parameter upon cycling.

The Measurements and the Data Processing Method. Due to the high precision required in this kind of measurements, a description of the technique used to prevent the introduction of systematic errors can be of interest.

In principle, the test did not present serious experimental difficulties, since the whole system (beam + cell + detector) was not submitted to any movement during the real-time measurement. To maximize the quantity of irradiated sample, the cell was placed so that the X-ray beam impinges on the membrane deposited on the aluminum foil collector under an incidence angle of 1°.

The diffraction signal reaching the detector was composed by the superposition of the diffractograms produced by the High-Density Poly-Ethylene (HDPE) cell walls (1), the electrolytic solution (2), the sample itself (3), and the Al foil (4). The contributions of (3) and (4) consisted of well-defined (and not overlapping) Debye−Scherrer rings; (1) gave the typical intensity distribution of a semicrystalline sample with two thin rings at low angles and a diffuse background elsewhere, while the contribution of (2) was just the diffuse halo of a liquid.

Also processing of the data is theoretically simple. Once the radial integration was carried out, so that the two-dimensional diffraction images are converted into mono-dimensional diffractograms, Miller indexes could be easily assigned to the Bragg peaks produced by the sample only. Since the crystalline lattice of $Li_{4/3}Ti_{5/3}O_4$ is cubic, the a parameter values could be obtained from just a single peak. In this way, so many independent samplings of the parameter could be obtained as the number of peaks having a sufficient intensity. Therefore, the a vs x curve could be described precisely on the base of a large set of data points.

However, the above-mentioned high geometrical stability of the system was not matched by an equivalent stability of the synchrotron X-ray beam. It is well-known that, unlike the laboratory sources, the intensity of a synchrotron beam is not constant and undergoes a decrease until the electron refill in the storage ring takes the intensity back to its initial value. In this case, long-lasting time-resolved measurements must be corrected for such an effect. This does not usually represent a major problem, because the beam intensity is monitored and the diffractograms can be normalized to it.

In the present case, instead, a secondary effect of the X-ray beam intensity decrease induced serious difficulties. The X-ray

beam produced in synchrotrons has a continuous energy spectrum ("white") that must be monochromatized to be used for this kind of diffraction measurements. The monochromator devoted to this role receives the whole white beam and diffracts one of the energetic components in the direction of the sample. According to the Bragg law, the selected energy is related to the value of the lattice parameter of the monochromator crystal. For this reason, the monochromator must be kept at constant temperature to contrast the heating effect of the high power white X-ray beam. This latter effect is dependent on the intensity of the synchrotron beam and varies with time. To solve this problem, a feedback system is used to guarantee a good thermal stability of the monochromator, and thus a stable monochromatic beam. However, when the electrons are re-injected in the synchrotron storage ring this method fails since the monochromator undergoes a rapid cooling due to the temporary absence of the radiation power and the beam energy results shifted at the restart. In ordinary experiments this effect is absolutely negligible, but in the present case even very small systematic errors may compromise the result.

The presence of extraneous Bragg reflections in the collected diffraction pattern, often considered an unavoidable inconvenience, was helpful in this case to solve the above-reported difficulties. In fact, the Bragg reflections of the HDPE cell container and of the aluminum current collector could be used as internal standards for data elaboration. By comparing their apparent shift (due to the beam energy fluctuations) with the shift of the titanate peaks (partially apparent and partially real), the residual real shift of the latter could be deduced.

Because of the cubic structure of the $Li_{4/3}Ti_{5/3}O_4$ compound, each of its Bragg peaks indeed provide an independent sampling of the lattice parameter. Therefore, it was possible either to calculate the parameter by a global fit of the pattern in the usual way, or to obtain as many values of it as the numbers of peaks present in the diffractogram. The latter choice offered two advantages.

The first is that nonlinear effect should be expected, since we operate in proximity of the detection limit of the image plate. In fact, it has to be remarked that the overall shift of each peak center of mass is a small fraction of a single pixel and, consequently, any minimal imperfection in the detection mechanism will produce a systematic error on the parameter value. If some detector region in which a peak may be placed exhibits a slightly anomalous behavior, the error will influence the final calculation of the lattice parameter. Instead, by analyzing peak by peak, the anomalies can be revealed and the peaks having anomalous behaviors discarded.

The second advantage stays in the possibility of adopting a very simple procedure that prevents errors that may compromise the final result and provides the parameter values (one for each peak) straightforwardly.

The procedure we suggest for processing data is based on the analytic structure of the relation between the scattering parameter q, on which the diffracted intensity depends, and the couple of variables E and ϑ (X-ray beam energy and half the diffraction angle). This relation can be written as

$$q = \alpha E \sin\vartheta \tag{1}$$

where α is constant (1.014 keV^{-1} $Å^{-1}$). In fact, by carrying out the logarithmic differential of the previous equation, the following is obtained:

$$\frac{\Delta q}{q} \cong \frac{\Delta E}{E} + \frac{\Delta\vartheta}{tg\ \vartheta}$$

where $\Delta q = q(t) - q(0)$, i.e., the displacement of q at time t with respect to its undisturbed initial value. Since the variation of the quantities involved is very small, this relation is almost exact. Applying it to a reference peak (for which $\Delta q = 0$), we have

$$\frac{\Delta E}{E} \cong -\frac{\Delta\vartheta_0}{tg\ \vartheta_0}$$

Therefore, the relative q shift of the peaks may be simply obtained by

$$\frac{\Delta q}{q} \cong \frac{\Delta\vartheta}{tg\ \vartheta} - \frac{\Delta\vartheta_0}{tg\ \vartheta_0} \tag{2}$$

However, it would be more convenient and straightforward to calculate the relative variation of the peak positions X, rather than that of the peak angle ϑ. Indeed, in this case, no uncertainty coming from the determination of the sample−detector distance R would be involved in the calculation.

From the geometric arrangement (see Figure 1)

$$X = R\ tg\ 2\vartheta$$

and in the same way as before,

$$\frac{\Delta X}{X} \cong \frac{\Delta tg\ 2\vartheta}{tg\ 2\vartheta} = 2\frac{\Delta\vartheta}{\sin 2\vartheta \cos 2\vartheta}$$

By comparison with eq 2, we obtain

$$\frac{\Delta q}{q} \cong \cos^2\vartheta\cdot\cos 2\vartheta\frac{\Delta X}{X} - \cos^2\vartheta_0\cdot\cos^2\vartheta_0\frac{\Delta X_0}{X_0}$$

so that a direct relation of the relative q-shift of each peak ($\Delta q/q$) with the variation in the positions of the same peak ($\Delta X/X$) and of the reference peak ($\Delta X_0/X_0$) can be found. The coefficients of the two $\Delta X/X$ terms in the right-hand side are constant and their values are practically unitary in the angular range of interest, so that can be neglected.

Finally, due to the relation between q and the lattice spacing d in a cubic crystal, that is $d = 2\pi/q$, the a value as a function of time can be gained:

$$a(t) = \frac{a(t=0)}{1 + \Delta q(t)/q}$$

where the time dependence has been rendered explicit.

Results and Discussion

In Figure 2 the complete sequence of the recorded diffractograms is reported as a function of the scattering parameter q. No visible changes in the patterns are detectable during cycling: neither new peak growth, nor shifts in peak position. Only performing a Non-Linear Least Square (NLLS) fit using a pseudo-Voigt profile function on all the patterns and for every single peak, we could detect a shift and calculate from that the a lattice parameter variation. As an example, we report in Figure 3 the results obtained by processing the 311 titanate peak position using no reference (curve a) and using as reference Al 311 peak (curve b) and HDPE1 (curve c). The first curve (a) shows sudden breaks exactly in correspondence with the synchrotron refill procedure and no evidence of any correlation with the cell voltage profile. Curves (b) and (c), on the other hand, show trends in phase with the galvanostatic cycling. However, it can be noticed that the (b) and the (c) curves look

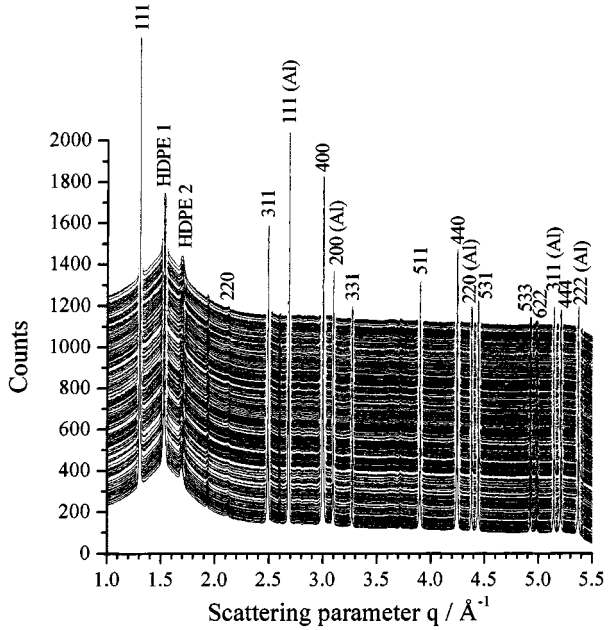

Figure 2. Sequence of the $Li_{4/3}Ti_{5/3}O_4$ diffraction patterns collected over two complete discharge−charge cycles. Each pattern was shifted upward for clarity reasons.

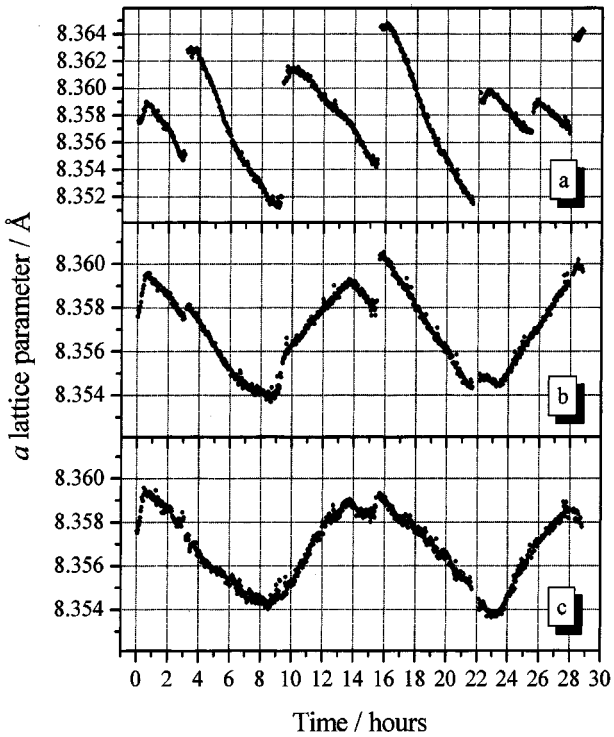

Figure 3. Lattice parameter evolution curves as a function of time obtained by processing the 311 titanate peak position, according to the discussion in the Experimental Section: (a) using no reference; (b) using as reference the Al 311 peak; (c) using as reference the HDPE1 peak.

different, the former still showing some influence from the synchrotron refill disturbance.

The reason for such an unexpected bad accuracy when aluminum is used as reference is most probably due to heating effects. In fact, the X-ray absorption of aluminum ($Z_{Al} = 13$) is expected to be higher than the one of HDPE (in which only C and H atoms are present). Furthermore, the current collector is a thin foil, i.e., it has a low thermal capacity, and it is conductive, so that it has a high thermal expansion coefficient. On the other hand, the cell container is much larger in dimensions, non conductive and made of HDPE, so that heating effects should be negligible and, even if they are not, they should not affect its structure.

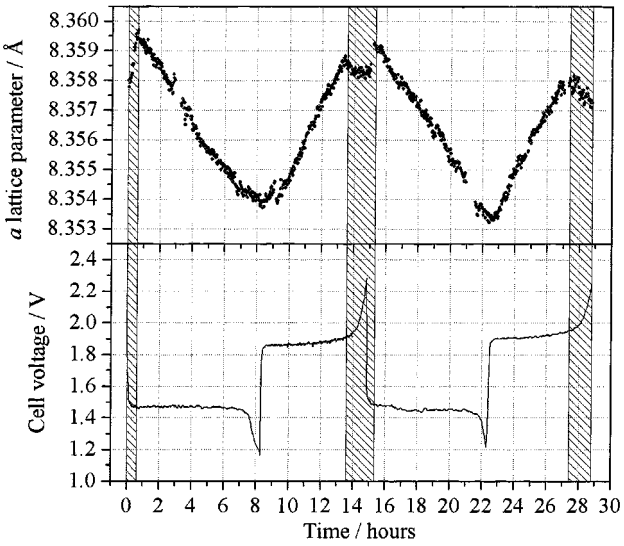

Figure 4. (Top) The curve of the *a* lattice parameter variation with time calculated by averaging the curves obtained by processing all the other major Bragg reflections. As in Figure 3c, the HDPE1 peak was used as reference. (Bottom) Cell voltage profile as a function of time. See text for discussion.

Every visible titanate peak, from 111 to 444, was fitted in the way reported above and 11 independent curves where obtained for the *a* parameter time evolution.

In Figure 4, the average of such curves is plotted as a function of cycling time, together with the cell voltage curve. The high noise and polarization of the cell voltage curve is due to the length of the cables connecting the cell (placed inside the experimental hutch) to the cycler and data acquiring computer (placed in the control cabin). The overall variation of the lattice parameter was confirmed to be less than 0.1%, as reported in previous works,[7,9] changing from 8.3596 to 8.3538 Å during the first cycle and from 8.3592 to 8.3532 Å during the second one.

Thanks to the unprecedented accuracy attainable by applying this procedure to in-situ diffraction studies of electrochemical cells, even the smallest details of the $a(t)$ curve could be observed. Indeed, the static geometry of the experimental setup, the very high statistical accuracy due to the full radial integration of the Debye−Scherrer rings, and the data processing based on the HDPE Bragg peaks used as inner standards (rather than on external parameters as sample-to-detector distance, X-ray beam energy, diffraction angles, etc.) allowed us to reach the resolution on *a* shown in Figure 4.

The most interesting feature is the unexpected slope variations in the *a* curve that occur at the beginning of the discharge (insertion) process and at the end of the charge (deinsertion), i.e., for small *x* values. It is to be noted, in fact, that the slope inversion shows a correspondence with the voltage curve only at the end of the discharge process, but not at the end of charge. This result was not expected because, in a two-phase process, the lattice parameters (related to peak positions) of the two phases remain unchanged, while the relative phase amount (related to peak intensities) changes from 0 to 100% or vice-versa. In the present case, being the two phases almost identical, the two contributions to diffraction of the two phases cannot be distinguished because their Bragg peaks overlap. As a

consequence, separated values for the a_1 and a_2 parameters of the two phases cannot be obtained but, rather, an average value that should change linearly as a function of the insertion degree as the galvanostatic cycling proceeds, according to the following equation:

$$\bar{a} = (1 - x)a_1 + xa_2$$

This behavior was observed only in the central part of the two cycles, in which the *a* curve show the expected "V" shaped trend, but not in the shaded regions reported in Figure 4. The most reasonable explanation for this evidence is inspired by what is discussed by Sharner et al.[7] The authors report that the initial $[Li]_{8a}[Li_{1/3}Ti_{5/3}]_{16d}[O_4]_{32e}$ phase can actually insert small amounts of lithium ions as a solid solution. In this view, the insertion process can be divided in two consecutive steps:

$$Li_{4/3}Ti_{5/3}O_4 + \delta Li^+ + \delta e^- \Leftrightarrow Li_{4/3+\delta}Ti_{5/3}O_4 \quad \text{(one phase)} \quad \text{(a)}$$

$$Li_{4/3+\delta}Ti_{5/3}O_4 + (1 - \delta)Li^+ + (1 - \delta)e^- \Leftrightarrow Li_{7/3}Ti_{5/3}O_4 \quad \text{(two phases)} \quad \text{(b)}$$

In mono-phase domains (eq a), represented in shaded regions in Figure 4, the lattice parameter value increases, as expected, with lithium insertion and decreases with deinsertion. The unshaded areas, on the other hand, are ruled by the two-phase process (eq b), as confirmed by the voltage plateaus and, in this case, the experimental values follow the above equation for $\bar{a}$. In ref 7, the authors report a δ value of 0.03, suggesting that such a value may be dependent on the powder surface area. We found higher values for δ, which ranges from about 0.05 (during the discharge process) to about 0.17 (during the charge process).

Finally, from the analysis of the curve in Figure 4, some information on the structural reversibility of this material could be obtained. In our previous work on the laboratory EDXD study of $Li_{4/3}Ti_{5/3}O_4$,[9] we conjectured the presence of partially irreversible effects occurring in the first cycles, like the ones observed for all other insertion compounds. Such a phenomenon seems to be confirmed by little differences (above the statistical noise) between the two cycles.

Conclusions

The use of a high-energy synchrotron beam allowed us to perform a highly accurate in-situ study on the structural evolution of the $Li_{4/3}Ti_{5/3}O_4$ insertion compound and to obtain a very dense-sampled curve of the lattice parameter change upon cell cycling. The results confirmed a very small variation of the lattice parameter of about 0.006 Å (i.e., ~0.07%) and showed an unexpected behavior in the initial and final parts of the two discharge−charge cycles. This evidence was attributed to the presence of two different insertion domains, a mono-phase domain in which the structure expands upon insertion and a following two-phase domain in which the structure contracts.

References and Notes

(1) Johnston, D. C.; Prakash, H.; Zachariasen, W. H.; Viswanathan, R. *Mater. Res. Bull.* **1973**, *8*, 777.
(2) Ohzuku, T.; Ueda, A.; Yamamoto, N.; Iwakoshi, Y. *J. Power Sources* **1995**, *54*, 99.
(3) Panero, S.; Satolli, D.; Salomon, M.; Scrosati, B. *Electrochem. Commun.* **2000**, *2*, 810.
(4) Ohzuku, T.; Ueda, A.; Yamamoto, N. *J. Electrochem. Soc.* **1995**, *142* (5), 1431.
(5) Dalton, M.; Tunstall, D. P.; Todd, J.; Arumugam, S.; Edwards, P. P. *J. Phys.: Condens. Matter* **1994**, *6*, 8859.
(6) Kartha, J. P.; Tunstall, D. P.; Irvine, J. T. S. *J. Solid State Chem.* **2000**, *152*, 397.
(7) Sharner, S.; Weppner, W.; Schmid-Beurmann, P. *J. Electrochem. Soc.* **1999**, *146* (3), 857.
(8) Ronci, F.; Scrosati, B.; Rossi Albertini, V.; Perfetti, P. *Electrochem. Solid State Lett.* **2000**, *3* (4), 174.
(9) Panero, S.; Reale, P.; Ronci, F.; Scrosati, B.; Perfetti, P.; Rossi Albertini, V. *Phys. Chem. Chem. Phys.* **2001**, *3*, 845.
(10) Rossi Albertini, V.; Perfetti, P.; Ronci, F.; Scrosati, B. *Chem. Mater.* **2001**, *13*, 450.
(11) Rossi Albertini, V.; Perfetti, P.; Ronci, F.; Reale, P.; Scrosati, B. *Appl. Phys. Lett.* **2001**, *79*, 27.